Australasian Physical & Engineering Sciences in Medicine (2019) 42:1069–1079
https://doi.org/10.1007/s13246-019-00804-y

SCIENTIFIC PAPER

Analysis of the disc pressure of the upper thoracic spine using pressure-sensitive film: an experimental study in porcine model—implications for scoliosis progression

Zhao Meng[1] · Chen Wang[1] · Xuzhao Guo[1] · Wei Chen[2] · Wenyuan Ding[3]

Received: 11 October 2018 / Accepted: 30 September 2019 / Published online: 15 October 2019

Abstract
There has been few studies focusing on the disc pressure of the upper thoracic spine and it still lacks the quantitative pressure measurement of each spinal disc segment. The aim of this study was to study the pressure changes of intervertebral disc in porcine upper thoracic spine using pressure-sensitive film. Twelve porcine thoracic motion segments were harvested and successively loaded with vertical loads of 100 N, 150 N, and 200 N during 5° of anterior flexion, 5° of posterior extension and 5° of lateral bending. The resulting pressure values were measured. During anterior flexion, the anterior annulus of all segments at all loads showed higher mean pressure values than those during vertical compression, whereas the posterior annulus did not show higher mean values. During posterior extension, the anterior annulus of all segments showed lower mean pressure values than those during vertical compression, whereas the posterior annulus did not show lower mean pressure values. During lateral bending, the annulus of all segments showed higher mean pressure values than those during vertical compression. The posterior thoracic vertebra plays an important role in the motion of the upper thoracic vertebral segment and pressure distribution. During lateral bending, the concave side pressure of the annulus increases obviously, suggesting that asymmetrical force is a contributory factor for scoliosis progression.

Keywords Upper thoracic spine · Pressure sensitive film · Pressure · Biomechanical analysis · Scoliosis

Introduction

Changes in normal spine curvature can cause specific spinal deformities, of which spinal scoliosis is one of the most complex three-dimensional deformities [1]. However, the etiology of scoliosis remains unclear. Current studies consider it as a multifactorial process, including changes in gene, hormone, thrombocyte, growth and development, as well as biomechanics [2–4]. However, after the initiation of scoliosis, biomechanics will be the main factor affecting the disease progress, especially the vertebrae imbalance [5–7].

Biomechanical evaluation of spinal stability can help to better understand the optimal surgical treatments for scoliosis. Previous studies regarding the biomechanical effects of scoliosis mainly focus on the thoracolumbar spine, lower thoracic spine, and lumbar spine [8–17]. To our knowledge, there have been few biomechanical researches regarding the upper thoracic spine, because the upper thoracic spine has a unique and complex physiologic structure. Meanwhile, upper thoracic scoliosis is common in clinics, and therefore exploring the biomechanical characteristics of the upper thoracic spine will help to develop new surgical modalities and more effectively treat upper thoracic scoliosis. Finite element analysis is currently the most advanced biomechanical method, because it can subdivide the spinal structure, simulate the role of each spinal structure in motion, and may predict scoliosis progress [18–22]. Healy et al. evaluated thoracic spinal stability after common surgical decompressive procedures in thoracic spines with intact sternocostovertebral articulations [23]. Little et al. compared the

✉ Zhao Meng
mengzhao88@yeah.net

[1] Department of Orthopaedics, Children's Hospital of Hebei Province, No. 133, South Jianhua Street, Shijiazhuang 050031, People's Republic of China

[2] Department of Traumatology Orthopaedics, The Third Affiliated Hospital of Hebei Medical University, Shijiazhuang, People's Republic of China

[3] Department of Spinal Surgery, The Third Affiliated Hospital of Hebei Medical University, Shijiazhuang, People's Republic of China

biomechanics of costotransverse process screw fixation with those of pedicle screw fixation in a cadaveric model of the upper thoracic spine [24]. However, it still lacks the quantitative pressure measurement of each spinal disc segment.

Edwards et al. [8] examined the distribution of stress across the area of the intervertebral disc using pressure probes. However, its results are only from certain points and also not intuitive [25]. Pressure-sensitive film can accurately measure the pressure range and distribution over a contact area. It is usually composed of two polyurethane composite films: a microcapsule layer (A-film) and a color-developing layer (C-film). To date, it has seen widely applied for studying the contact mechanics in artificial joints [26–29]. To our knowledge, there have been few reports regarding biomechanical studies of the upper thoracic spine using pressure sensitive-film.

Immature pigs are usually used as animal models to test the spinal internal fixation system for scoliosis modeling, because they have a similar anatomical structure to humans and their growth cycle is suitable for disease progress research [30–32]. In this study, we investigated the pressure change and biomechanical characteristics of each spinal level of the upper thoracic spine in immature pigs during vertical load, 5° of anterior flexion, 5° of posterior extension, and 5° of lateral bending using pressure-sensitive film.

Methods

Specimen preparation

Twelve fresh-frozen female porcine cadaveric spine specimens were utilized in this study. The age of the mini-pigs ranged from 6 to 8 weeks with scoliosis growth potential. The mean weight of the specimens was 8.3 kg (ranging from 6 to 10 kg). Immature pigs were chosen because they are the most approximate animal model with respect to size and shape of the human vertebra [30–32]. One difference is that the vertebral bone density in pigs is higher than that of the human vertebra; however, we are planning to study the variation trend of disc stress; hence, this difference would not affect our results. Before biomechanical testing, computed tomography scans of each specimen were carried out to exclude the possibility of deformity, tumors, and fractures. Six thoracic motion segments were obtained from six of the specimens including T1–T2, T3–T4, T5–T6 and T7–T8 and another six thoracic motion segments were obtained from the remaining specimens including T2–T3, T4–T5, T6–T7 and T8–T9 segments. All the specimens were sealed in polyethylene film and stored in a freezer at − 20 °C. To prepare for the test, the specimens were taken out and thawed at 3 °C for 12 h. After thawing, all the thoracic motion segments were embedded in self-curing denture acrylic (Dental Materials Factory of Shanghai Medical Instruments Co., Ltd, China) with upper and inferior ends of thickness 1.5 cm (Fig. 1) and placed perpendicular to the ground. Thereafter, the motion segment was mounted on a CSS-44020 biomechanical test machine (Changchun Research Institute for Testing Machines, Changchun, Jilin Province, China). A vertical load of 300 N [25] was applied to each segment for 15 min to reduce the hyper-hydration of the intervertebral disc. After dissecting the entire intervertebral disc in the transverse plane from anterior to posterior, the pressure-sensitive film (Prescale measurement film, Super Low Pressure, Fuji film Co. Ltd, Tokyo, Japan), wrapped in a plastic bag, was inserted in the intervertebral disc. During the process of disc dissection, care should be taken to avoid the injuries to the articular process, intact anterior and posterior longitudinal ligaments. The film can bear pressure in the range of 0.5 to 2.5 MPa. Prior to placement, the film was cut to an appropriate shape in order to match the intervertebral disc. We estimated the required film size from the size of the disc adjacent to the target dissected segment. The top of the film was cut into a thin and sharp shape, whereas the inferior part of the film was cut into a gradually widening shape (Fig. 2), to facilitate insertion into the dissected intervertebral disc. Before the formal experiments, we performed preliminary loading by using a compressive load of 200 N for three successive times 15 min intervals to completely eliminate the influence of the viscoelasticity of the specimens. The reason that we selected the load of 200 N for 15 min was because this load condition can completely eliminate the viscoelasticity and acquired clear pressure-sensitive films in our preliminary experiments [25, 33]. The motion segments were then successively loaded with 100 N, 150 N, and 200 N (approximately half of the body weight of an adult) perpendicular to the ground (Fig. 3a). The loading rate was set at

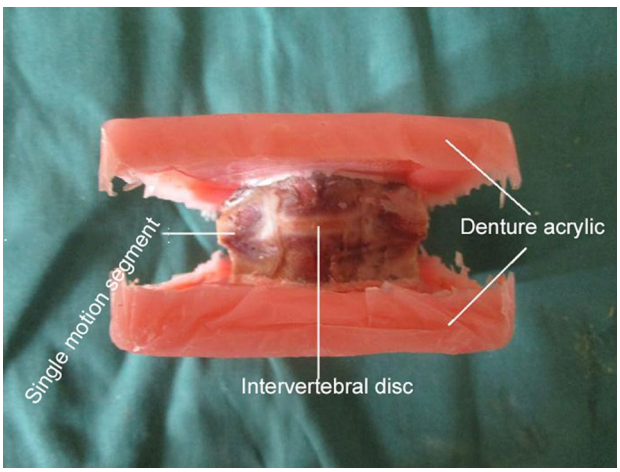

Fig. 1 Thoracic motion segments were embedded in self-curing denture acrylic with upper and inferior ends of thickness 1.5 cm

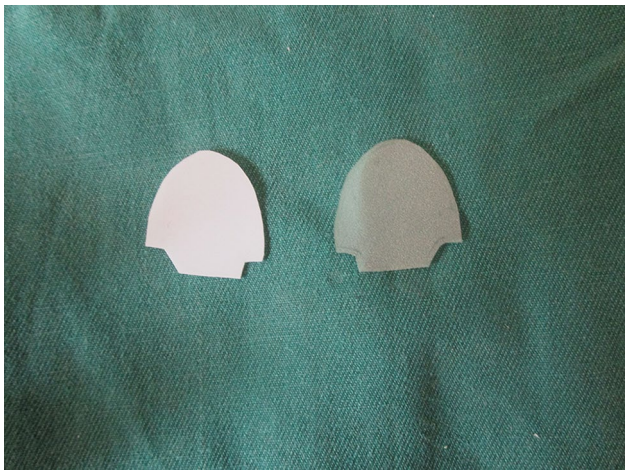

Fig. 2 Shape of film used in this study. The top of the film was cut into a thin and sharp shape, whereas the inferior part of the film was cut into a gradually widening shape

50 N/s according to our multiple preliminary experiments, which show that this loading rate can effectively prevent pressure-sensitive film from sliding in the intervertebral disc and thus help to acquire clear pressure-sensitive films. For each specimen, the entire load sequence test was repeated three times; if the results of these three trials were similar, the mean value was selected. Under extreme conditions, if the three trials yield uneven loading results, a vertical load of 300 N for 15 min and a compressive load of 200 N for 15 min should be applied on each segment to eliminate the influences of the hyper-hydration of the intervertebral disc and viscoelasticity of the specimens [25, 33]. In this study, no such extreme conditions occurred. The film remained in place for 2 min in order to obtain more homogeneous images. Thereafter a wedge-shaped 5° inclined plane made using self-curing denture acrylic (Fig. 3b) was placed between the test machine and motion segment to stimulate stress profiles during 5° of anterior flexion, 5° of posterior extension, and 5° of lateral bending [8]. The test process was identical to the purely compressive loading stimulation process described above. All these procedures described above were performed at a temperature of 20 °C and relative humidity of 44%.

The contact pressures were measured with a prescale densitometer (FPD-305E, Fuji Photo Film Co., Tokyo, Japan) and a prescale pressure reader (FPD-306E) designed for use with the film. The densitometer was precalibrated to measure color development density. It automatically adjusted for atmospheric conditions, including temperature and humidity, at the time of testing. The pressure reader converted the color density measurement to a pressure reading in megapascals (MPa). The contact pressure of each film was measured by using manual tracing in 1-mm increments. Each measurement was repeated twice by one researcher and the mean value was quantified. The approximate numbers of stress measurements that contributed to each reported value of the anterior annulus, posterior annulus, and annulus during lateral bending were 20–30, 10–20, and 15–25, respectively.

In this study, we quantified the pressure values of the three regions (anterior annulus, posterior annulus, and entire annulus) of the intervertebral disc from the measured profiles at each load condition. According to the three-column theory, the anterior two thirds of the disc was assumed to be the anterior annulus, and the posterior

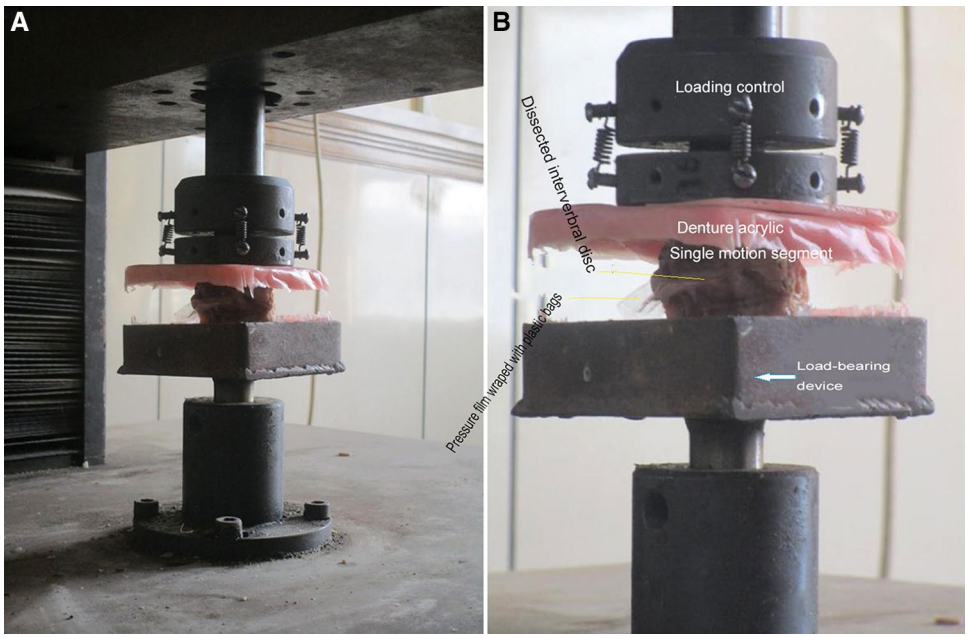

Fig. 3 **a** The motion segments were successively loaded with 100 N, 150 N, and 200 N during vertical position. **b** A wedge-shaped slope 5° inclined plane made using self-curing denture acrylic was placed between the test machine and motion segment to stimulate stress profiles during different positions

one third was assumed to be the posterior annulus. McAfee et al. [34] proposed the concept of the three-column spine, i.e., (1) the anterior column consists of the anterior two thirds of the vertebral body, anterior annulus, and anterior longitudinal ligament; (2) the middle column consists of the posterior longitudinal ligament, posterior annulus, and posterior one third of the vertebral body; and (3) the posterior column consists of the facet-joint capsules, ligamentum flavum, osseous neural arch, supraspinous ligament, interspinous ligament, and articular processes. During the lateral bending, the measured profiles were taken from the half of the curved concave sides of the entire annulus (Fig. 4).

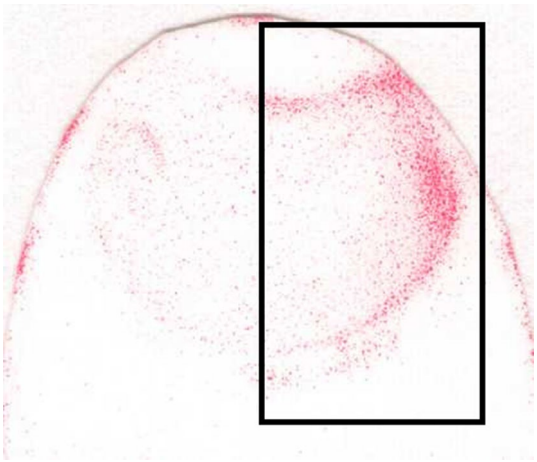

Fig. 4 During the lateral bending, the measured profiles were taken from the half of the curved concave sides of the entire annulus

Statistical analysis

The data analysis was performed using SPSS 13.0 (SPSS Inc., Chicago, IL, USA). The data were expressed as mean ± standard deviation (SD). A Multi-sample means comparison was performed using one-way analysis of variance (ANOVA) to analyze the pressure values of different segments at a load of 100 N, 150 N, and 200 N during different conditions, and the multiple comparisons were determined by using the LSD test or Dunnett T3 test when the variance was heterogeneous. The differences were considered statistically significant when $P < 0.05$.

Results

Stress data of spinal levels

The stress data of each spinal level of the upper thoracic vertebrae under vertical loads of 100 N, 150 N, and 200 N are shown in Table 1. Statistical tests showed that there were statistically significant differences regarding the mean pressure among the different loads at the anterior, posterior, and entire annulus of all spinal levels. Moreover, the mean pressure values of the anterior, posterior and entire annulus of all spinal levels all showed an overall tendency to increase with the increasing load (Table 1).

In addition, we found that the pressure increases of posterior annulus (posterior column) and entire annulus of all spinal levels between the loads of 150 N and 200 N was smaller than those between 100 and 150 N (Table 1).

Table 1 Pressures values (MPa) of the anterior, posterior, and entire annulus of each segment under vertical loads of 100 N, 150 N, and 200 N (means ± SD)

Segments	SA100	SA150	SA200	SP100	SP150	SP200	S100	S150	S200
T1–2	0.35 ± 0.18	0.45 ± 0.09	0.55 ± 0.04	1.00 ± 0.08	1.81 ± 0.11[a]	2.11 ± 0.24[b,c]	0.55 ± 0.12	1.10 ± 0.08[a]	1.24 ± 0.10[b,c]
T2–3	0.37 ± 0.17	0.57 ± 0.11[a]	0.71 ± 0.06[c]	0.62 ± 0.06	1.33 ± 0.11[a]	1.64 ± 0.08[b,c]	0.46 ± 0.11	0.95 ± 0.10[a]	1.03 ± 0.09[c]
T3–4	0.41 ± 0.15	0.67 ± 0.10[a]	0.82 ± 0.05[b,c]	0.38 ± 0.04	0.88 ± 0.07[a]	1.10 ± 0.20[b,c]	0.38 ± 0.08	0.82 ± 0.06[a]	0.87 ± 0.06[c]
T4–5	0.49 ± 0.12	0.77 ± 0.06[a]	0.87 ± 0.02[c]	0.24 ± 0.03	0.64 ± 0.08[a]	0.84 ± 0.07[b,c]	0.37 ± 0.09	0.78 ± 0.09[a]	0.81 ± 0.05[c]
T5–6	0.56 ± 0.13	0.79 ± 0.09[a]	0.87 ± 0.06[c]	0.22 ± 0.03	0.61 ± 0.05[a]	0.79 ± 0.07[b,c]	0.45 ± 0.04	0.75 ± 0.08[a]	0.81 ± 0.05[c]
T6–7	0.61 ± 0.12	0.78 ± 0.16	0.99 ± 0.22[c]	0.27 ± 0.04	0.66 ± 0.03[a]	0.83 ± 0.05[b,c]	0.51 ± 0.02	0.76 ± 0.09[a]	0.95 ± 0.13[b,c]
T7–8	0.61 ± 0.12	0.81 ± 0.18	1.11 ± 0.38	0.384 ± 0.04	0.70 ± 0.07[a]	1.02 ± 0.08[b,c]	0.53 ± 0.03	0.78 ± 0.09[a]	1.11 ± 0.17[b,c]
T8–9	0.58 ± 0.08	0.85 ± 0.18[a]	1.28 ± 0.51	0.502 ± 0.06	0.93 ± 0.10[a]	1.44 ± 0.09[b,c]	0.55 ± 0.04	0.97 ± 0.10[a]	1.39 ± 0.22[b,c]

SA100 average pressure values of anterior annulus at a load of 100 N, *SA150* average pressure values of anterior annulus at a load of 150 N, *SA200* pressure values of the anterior annulus under a load of 200 N, *SP100* average pressure values of the posterior annulus under a load of 100 N, *SP150* average pressure values of the posterior annulus under a load of 150 N, *SP200* average pressure values of the posterior annulus under a load of 200 N, *S100* average pressure values of the entire annulus under a load of 100 N, *S150* average pressure values of the entire annulus at a load of 150 N, *S200* average pressure values of the entire annulus under a load of 200 N

[a]Versus SA100 or SP100 or S100, $P < 0.05$

[b]Versus SA150 or SP150 or S150, $P < 0.05$

[c]Versus SA100 or SP100 or S100, $P < 0.05$

Stress data of spinal levels during 5° of anterior flexion

The stress data of each spinal level of the upper thoracic vertebrae under loads of 100 N, 150 N, and 200 N during 5° of anterior flexion are shown in Table 2. Statistical tests showed that there were statistically significant differences regarding pressure values among the different loads at the anterior and posterior annulus of all spinal levels. Moreover, the mean pressure values at the anterior and posterior annulus of all spinal levels showed an overall tendency to increase with the increasing load (Table 2) during 5° of anterior flexion. Furthermore, the mean pressure values at the anterior and posterior annulus of all spinal levels under the load of 200 N was all statistically significantly higher than those under 100 N ($P < 0.05$).

Stress data of spinal levels during 5° of posterior extension

The stress data of each spinal level of the upper thoracic vertebrae under loads of 100 N, 150 N, and 200 N during 5° of posterior extension are shown in Table 3. With regard to the anterior annulus, there was no consistent variation regarding the mean pressure values of spinal levels among the different loads (Table 3), particularly in the T2-3 and T3-4 segments.

With regard to the posterior annulus, statistical tests showed that there were statistically significant differences regarding pressure values of all spinal levels among the different loads. In addition, the mean pressure values at the posterior annulus of all spinal levels showed a tendency to increase with the increasing load (Table 3) during 5° of posterior extension. Furthermore, the mean pressure values at the posterior annulus of all spinal levels under the load of 200 N were all statistically significantly higher than those under 100 N (all $P < 0.05$), and those under 150 N (except for the T2–3 segment).

Stress data of spinal levels during 5°of lateral bending

The stress data of each spinal level of the upper thoracic vertebrae under loads of 100 N, 150 N, and 200 N during 5° of lateral bending are shown in Table 4. Statistical tests showed that there were statistically significant differences regarding the mean pressure values at the annulus of all spinal levels among the different loads. Moreover, the mean pressure values at the annulus of all spinal levels showed a tendency to increase with the increasing load under 5° of lateral bending (Table 4).

Influence of posture on disc stresses

For the motion analysis, we found that the mean pressure at the anterior annulus of all spinal levels during vertical compression under 100 N, 150 N, and 200 N loads had relatively lower values compared to those during anterior flexion, but higher values compared to those during posterior extension, although these differences were not sill statistically significant (Fig. 5).

Table 2 Pressure values of the anterior and posterior annulus of each segment under loads of 100 N, 150 N, and 200 N during 5° of anterior flexion (means ± SD)

Segments	AA100	AA150	AA200	AP100	AP150	AP200
T1–2	0.51 ± 0.06	0.65 ± 0.06[a]	0.98 ± 0.17[b,c]	0.68 ± 0.10	1.15 ± 0.13[d]	1.93 ± 0.12[e,f]
T2–3	0.61 ± 0.08	0.82 ± 0.04[a]	1.26 ± 0.08[b,c]	0.44 ± 0.07	0.83 ± 0.07[d]	1.42 ± 0.05[e,f]
T3–4	0.71 ± 0.09	0.95 ± 0.03[a]	1.41 ± 0.04[b,c]	0.30 ± 0.03	0.63 ± 0.05[d]	0.98 ± 0.13[e,f]
T4–5	0.78 ± 0.07	0.99 ± 0.08[a]	1.47 ± 0.08[b,c]	0.19 ± 0.03	0.60 ± 0.02[d]	0.86 ± 0.06[e,f]
T5–6	0.78 ± 0.11	0.91 ± 0.05	1.41 ± 0.17[b,c]	0.20 ± 0.06	0.62 ± 0.02[d]	0.89 ± 0.08[e,f]
T6–7	0.79 ± 0.18	1.02 ± 0.27	1.41 ± 0.47[c]	0.31 ± 0.07	0.64 ± 0.06[d]	0.90 ± 0.12[e,f]
T7–8	0.82 ± 0.23	1.101 ± 0.45	1.69 ± 0.54[b,c]	0.44 ± 0.04	0.74 ± 0.14[d]	1.11 ± 0.07[e,f]
T8–9	0.89 ± 0.27	1.115 ± 0.39	1.67 ± 0.58[b,c]	0.54 ± 0.03	1.01 ± 0.10[d]	1.50 ± 0.11[e,f]

AA100 average pressure values of the anterior annulus under a load of 100 N during 5° of anterior flexion, *AA150* average pressure values of the anterior annulus under a load of 150 N during 5° of anterior flexion, *AA200* pressure values of the anterior annulus under a load of 200 N during 5° of anterior flexion, *AP100* average pressure values of the posterior annulus under a load of 100 N during 5° of anterior flexion, *AP150* average pressure values of the posterior annulus under a load of 150 N during 5° of anterior flexion, *AP200* average pressure values of the posterior annulus under a load of 200 N during 5° of anterior flexion

[a]Versus AA100, $P < 0.05$

[b]Versus AA150, $P < 0.05$

[c]Versus AA100, $P < 0.05$

[d]Versus AP100, $P < 0.05$

[e]Versus AP150, $P < 0.05$

[f]Versus AP100, $P < 0.05$

Table 3 Pressure values of the anterior and posterior annulus of each segment under loads of 100 N, 150 N, and 200 N during 5° of posterior extension (means ± SD)

Segments	RA100	RA150	RA200	RP100	RP150	RP200
T1–2	0.17 ± 0.10	0.18 ± 0.08	0.24 ± 0.04	1.31 ± 0.07	2.09 ± 0.12[d]	3.00 ± 0.18[e,f]
T2–3	0.17 ± 0.08	0.25 ± 0.11	0.22 ± 0.03	0.91 ± 0.11	1.43 ± 0.20[d]	1.99 ± 0.49[f]
T3–4	0.19 ± 0.06	0.34 ± 0.11	0.24 ± 0.06[b,c]	0.54 ± 0.14	0.92 ± 0.27[d]	1.29 ± 0.42[e,f]
T4–5	0.19 ± 0.06	0.33 ± 0.04[a]	0.34 ± 0.05[c]	0.31 ± 0.06	0.78 ± 0.19[d]	1.04 ± 0.21[e,f]
T5–6	0.25 ± 0.03	0.28 ± 0.07	0.47 ± 0.05[b,c]	0.21 ± 0.09	0.64 ± 0.14[d]	0.92 ± 0.14[e,f]
T6–7	0.45 ± 0.03	0.51 ± 0.10	0.62 ± 0.04[b,c]	0.23 ± 0.09	0.55 ± 0.06[d]	0.88 ± 0.06[e,f]
T7–8	0.55 ± 0.12	0.64 ± 0.23	0.72 ± 0.11	0.34 ± 0.12	0.67 ± 0.11[d]	1.23 ± 0.15[e,f]
T8–9	0.40 ± 0.08	0.58 ± 0.20	0.77 ± 0.20[c]	0.55 ± 0.12	1.03 ± 0.12[d]	1.78 ± 0.07[e,f]

RA100 average pressure values of the anterior annulus under a load of 100 N during 5° of posterior extension, *RA150* average pressure values of the anterior annulus under a load of 150 N during 5° of posterior extension, *RA200* average pressure values of anterior annulus at a load of 200 N during 5° of posterior extension, *RP100* average pressure values of the posterior annulus under a load of 100 N during 5° of posterior extension, *RP150* average pressure values of the posterior annulus under a load of 150 N during 5° of posterior extension, *RP200* average pressure values of the posterior annulus under a load of 200 N during 5° of posterior extension

[a]Versus RA100, $P < 0.05$

[b]Versus RA150, $P < 0.05$

[c]Versus RA100, $P < 0.05$

[d]Versus RP100, $P < 0.05$

[e]Versus RP150, $P < 0.05$

[f]Versus RP100, $P < 0.05$

Table 4 Pressure values of the annulus of each segment under loads of 100 N, 150 N, and 200 N during 5° of lateral bending (means ± SD)

Segments	B100	B150	B200
T1–2	0.81 ± 0.08	1.39 ± 0.19[a]	1.61 ± 0.03[c]
T2–3	0.71 ± 0.08	1.12 ± 0.14a	1.57 ± 0.02[b,c]
T3–4	0.66 ± 0.04	1.10 ± 0.06[a]	1.51 ± 0.04[b,c]
T4–5	0.65 ± 0.02	1.10 ± 0.06[a]	1.41 ± 0.08[b,c]
T5–6	0.63 ± 0.03	1.01 ± 0.06[a]	1.26 ± 0.08[b,c]
T6–7	0.68 ± 0.03	1.08 ± 0.16[a]	1.37 ± 0.20[c]
T7–8	0.76 ± 0.02	1.38 ± 0.15[a]	1.86 ± 0.27[b,c]
T8–9	0.82 ± 0.04	1.44 ± 0.08[a]	1.98 ± 0.30[c]

B100 average pressure values of the annulus under a load of 100 N during 5° of lateral bending, *B150* average pressure values of the annulus under a load of 150 N during 5° of lateral bending, *B200* average pressure values of the annulus under a load of 200 N during 5° of lateral bending

[a]Versus B100, $P < 0.05$

[b]Versus B150, $P < 0.05$

[c]Versus B100, $P < 0.05$

With regard to the motion analysis of the mean pressure at the posterior annulus of all spinal levels, we find that the mean pressure at the posterior annulus during posterior extension under 100 N, 150 N, and 200 N loads showed increased values at certain spinal levels (such as the T1–2, T2–3,T3–4,T4–5, and T8–9 segments under a load of 100 N), but decreased values at other spinal levels (such as the T5–6, T6–7, T7–8 segments under a load of 100 N) compared to those during vertical compression (Fig. 6). In addition, we found that the mean pressure at the posterior annulus during anterior flexion under of 100 N, 150 N, and 200 N loads showed a decreased tendency at certain spinal levels, but increased tendency at other spinal levels compared to those during vertical compression.

With regard to the motion analysis of the mean pressure at the annulus of all spinal levels under of 100 N, 150 N and 200 N loads, we found that the mean pressures at the annulus of all spinal levels during lateral bending was statistically significantly higher than those of the entire annulus of all spinal levels during vertical compression under all loads (Fig. 7) (all $P < 0.05$).

Discussion

Currently, two methods including pressure probe and pressure-sensitive film are available for measuring intradiscal stress directly in loaded cadaver discs. Pressure probe can measure the stress value of single point of the disc without causing damages to the annulus. However, it is associated with the difficulty in controlling the insertion depth. In addition, it can only measure pressure locally but not globally [25]. Pressure-sensitive film can intuitively display the pressure characteristics of each segment in the upper thoracic and lumbar spine [27], which has the main force region centered on the annulus and nucleus. Using this approach, we

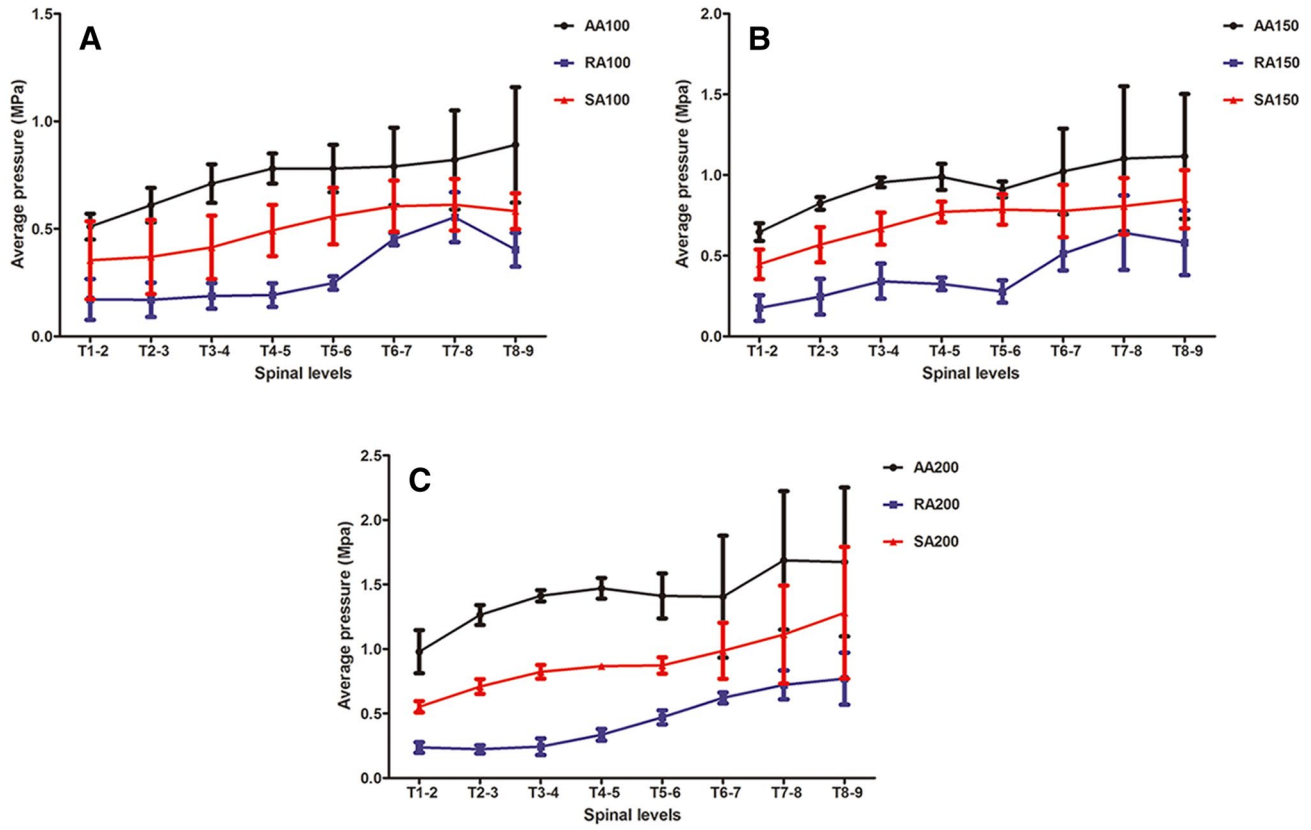

Fig. 5 The mean pressure at the anterior annulus of all spinal levels during vertical compression under 100 N, 150 N, and 200 N loads had relatively lower values compared to those during anterior flexion, but higher values compared to those during posterior extension, although these differences were not significant

can observe the force conditions of the entire annulus. In this study, we analyzed the mean pressure at the anterior and posterior annulus because they best reflect the load characteristics of the upper thoracic spine. In order to ensure the stability that pressure-sensitive films needed, we adopted a specimen fixation method similar to that used in a previous study by Adams et al. [25], i.e., a single motion segment was embedded in self-curing denture acrylic. This method has been widely used for measuring intervertebral disc pressure. In addition, the CSS biomechanics test machine employed in this study has a mold that can be used for fixing the vertebral body and load control component. By selecting a simple motion segment, the stability of pressure-sensitive film on the intervertebral disc can be guaranteed. It should be emphasized that we will not get stable stress images if the stability of the pressure-sensitive film cannot be guaranteed, thus we had performed a lot of preliminary experiments prior to the formal experiments to ensure the stability of the pressure-sensitive films within the intervertebral disc.

Previously, lumbar specimens were commonly used to study intervertebral disc pressures. Adams et al. [25] measured the stress distribution within cadaveric intervertebral discs during vertical load and found that the stress distribution varied with the lumbar level. In addition, they also found that the pressure of the anterior annulus at L1-2 was higher than that of the posterior annulus, and that the posterior annulus was affected more than the anterior annulus at L2-3, L3-4, and L4-5. Gay et al. [11] evaluated the reliability of stress profilometry measurements in the anterior, posterior, and nucleus regions of cadaveric lumbar discs, and found that the spinal level affect the resulting stress. Adams et al. tested the hypothesis that backward bending of the lumbar spine could reduce compressive stresses within the lumbar intervertebral discs and concluded that the posterior annulus could be stress-shielded by the neural arch in extended postures, but the effect was variable [35]. The aforementioned reports mainly focused on lumbar vertebrae and the results of the stress of the vertebral arch in lumbar vertebrae were not always obvious and varied under different conditions. In this study, we focused on the stress characteristics of the upper thoracic spine. In comparison to lumbar vertebrae, upper thoracic vertebrae will withstand more pressure. To our knowledge, it still lacks the quantitative pressure measurement of each spinal disc segment. In

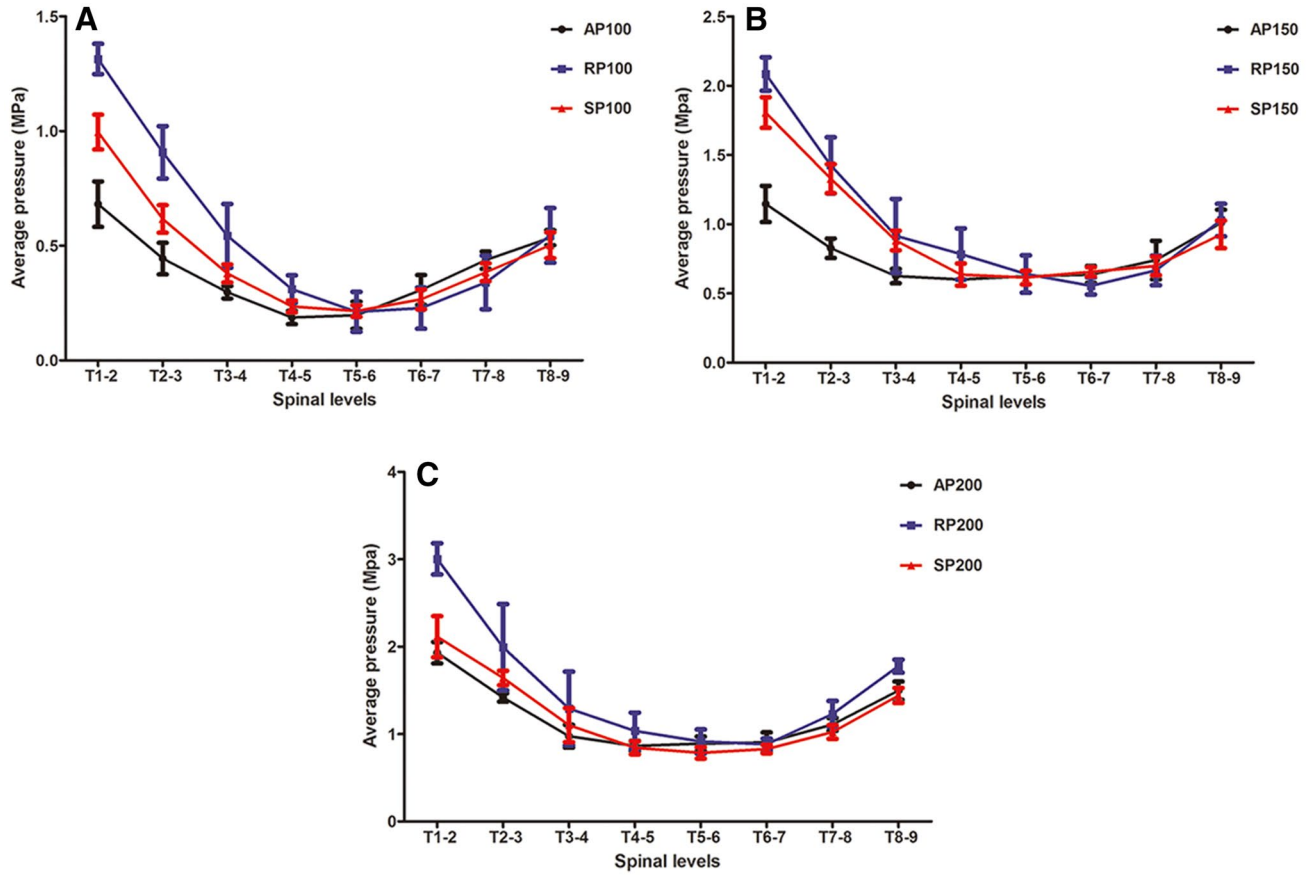

Fig. 6 The mean pressure at the posterior annulus during posterior extension under 100 N, 150 N, and 200 N loads showed increased values at certain spinal levels (such as the T1–2, T2–3, T3–4, T4–5, and T8–9 segments under a load of 100 N), but decreased values at other spinal levels (such as the T5–6, T6–7, and T7–8 segments under a load of 100 N) compared to those during vertical compression

this study, we found that the posterior annulus was more affected than that the anterior annulus at T1–2 and T2–3 under the vertical load of 100 N, and at T1–2, T2–3, T3–4, and T8–9 under the vertical loads of 150 N and 200 N. We observed that each spinal level had its stress characteristics, and varied with the increasing load. This may be related to the physiological curvature and structural features of the upper thoracic spine. With regard to the entire annulus, we found relatively stable increase ranges of pressure profiles at T7–8 and T8–9 with the increasing load, and smaller increase ranges of pressure profiles at other spinal levels of the upper thoracic spine. These may be due to the vertebral posterior region sharing part of the load, which becomes more pronounced with the increasing load, thereby resulting in the inconsistency between the increase range of the mean pressure in the entire annulus and the increase range of the load.

Gravity should not be ignored during the stress analysis of spinal scoliosis. Many spinal structures will respond to the mechanical load, thus resulting in corresponding pathological changes [2]. In this study, the pressure of the concave annulus in the intervertebral disc show clearly shows an increasing tendency with the increasing load during lateral bending. McMillan et al. [9] found that stress profiles obtained under different applied loads showed a similar distribution of stress within the disc and concluded that compressive stress at any location and direction increased in proportion to the applied load. It can be speculated that the spine will tolerate a greater load in patients with higher weight and the intervertebral disc will also bear relatively greater stress.

Under different motion conditions, gravity (under different loading) remains an import factor affecting spinal stress. During anterior flexion and posterior extension, the stress on the posterior annulus varied positively with the increasing load. With regard to the anterior annulus, the mean stress also varied positively with the increasing load during anterior flexion. On the contrary, there was no consistent variation regarding the mean pressure values of spinal levels under different loads during posterior extension, particularly in the T2–3 and T3–4 segments. These findings suggest that the middle and posterior column of the upper thoracic spine

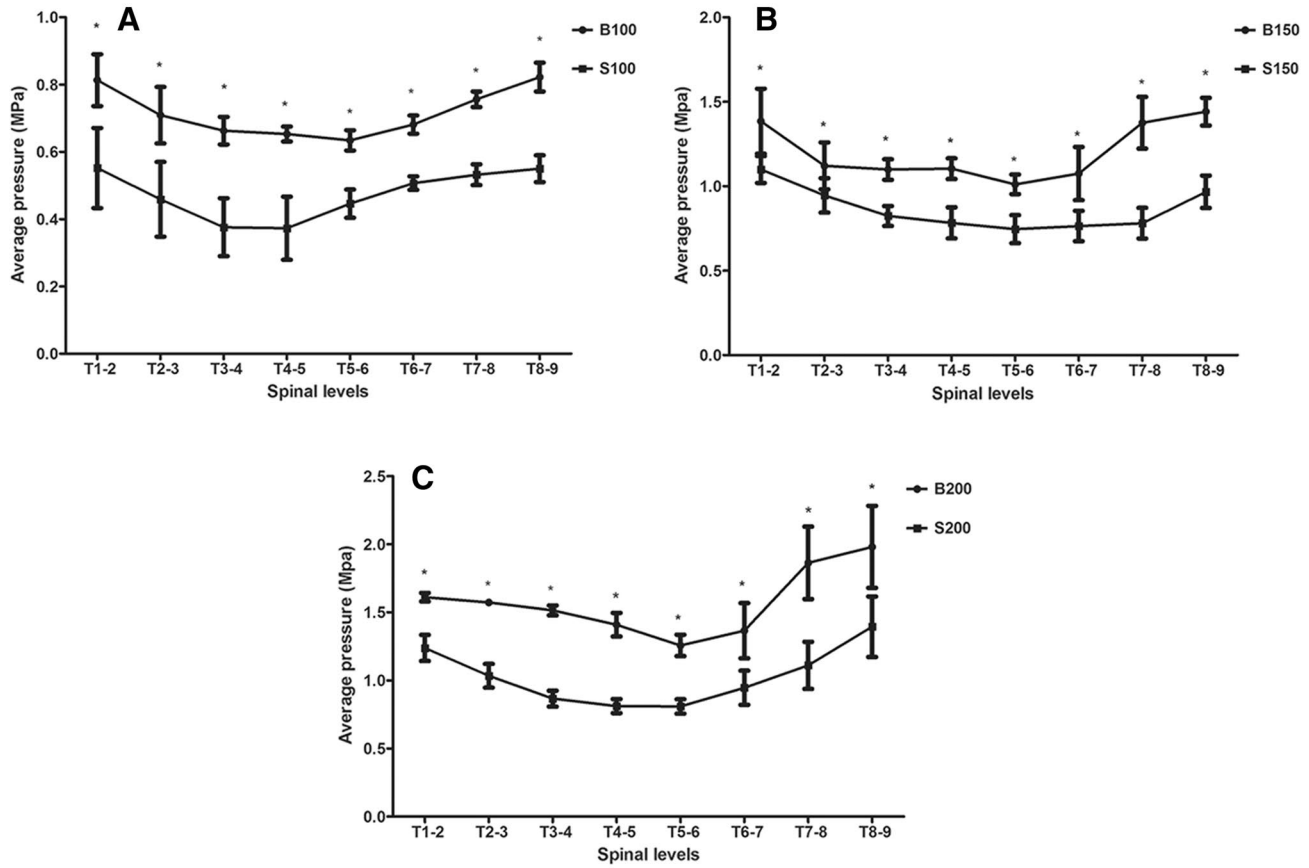

Fig. 7 The mean pressures at the annulus of all spinal levels during lateral bending were statistically significantly higher than those of the entire annulus of all spinal levels during vertical compression under all loads

tend to bear more load as the load increases, and the posterior regions of the spine plays an important role.

It is generally believed that increased stress can be observed at the anterior annulus during anterior flexion and the posterior annulus during posterior extension, and that decreased stress can be observed at the posterior annulus during anterior flexion and at the anterior annulus during posterior extension [8, 27, 36]. Edwards et al. [8] found that the highest values were measured at the posterior annulus during extension–compression. Steffen et al. [36] reported that the largest intradiscal pressure increase was observed at the posterolateral inner annular regions during posterior extension. However, all these reports focused on the lower thoracic spine, thoracolumbar spine, and lumbar segments. In the present biomechanical analysis of the upper thoracic spine, we obtained different results. We found increased stress at the anterior and posterior annulus during anterior flexion compared to those of vertical loading. In addition, we found that the anterior annulus showed decreased stress during posterior extension compared to vertical loading. However, certain spinal levels did not show obvious increased stress at the posterior annulus during anterior flexion compared to those during vertical compression. The unique stress characteristics of the upper thoracic spine are related to its physiological structure. According to the three-column theory [34], the lumbar intervertebral disc bears a majority of the interdiscal pressure within the spine. On the contrary, the upper thoracic spine bears relatively small interdiscal pressure owing to its small intervertebral disc and more posterior vertebral structures. During anterior flexion, the interdiscal pressure showed an overall increasing tendency due to the intervertebral disc moving anteriorly. Meanwhile, the interdiscal pressure showed an overall decreasing tendency due to the posterior column bearing a majority of the compressive stress during posterior extension.

Previous studies suggest that wedging of the intervertebral disc and centrum due to asymmetrical loading is a contributory factor for progress of scoliotic curves [37–40]. It is widely believed that this change of the intervertebral disc and centrum follows the Hueter-Volkmann principles. According to these, vertebral growth is mainly derived from the growth of the cartilage endplate and the morphological changes of scoliosis are highly associated with intervertebral disc stress. In this study,

we found that the concave side pressure of the annulus increases obviously during lateral bending and the mean pressure values at the annulus of all spinal levels showed a tendency to increase with the increasing load under lateral bending. In addition, we can intuitively observe the stress unbalance due to lateral bending. From the pressure-sensitive films and pressure data (shown in Table 4), we can observe the asymmetrical force. Long-term asymmetrical loading after the onset of scoliosis can cause the intervertebral disc and centrum wedging and thus is a contributory factor for scoliosis progress. In general, a large load or weight and lateral curvature will accelerate the scoliosis progress. The upper thoracic spine is the least affected by weight, which helps to explain the slow scoliosis progress. The role of the posterior structures in the upper thoracic spine sharing stress should not be ignored. Because the upper thoracic spine has unique stress characteristics compared to other spinal segments, improving the asymmetrical stress and reducing the load on the motion segments will be important methods for correcting spinal deformity.

This study has several limitations. This study only reported the final disc pressure under loading. Except the final disc pressure, study on biomechanics in such data as load–displacement curve, disc pressure-load curve should be further investigated. These data will be great beneficial for researchers on numerical modelling. However, limited to the biomechanical test machine and the use of test method of pressure-sensitive film, we are hard to collect these curves in this current study. However, to our knowledge, there has been no previous study focusing on the disc pressure of the upper thoracic spine and it still lacks the quantitative pressure measurement of each spinal disc segment. Pressure-sensitive film can intuitively display the pressure characteristics of each segment in the upper thoracic and lumbar spine (25), which has the main force region centered on the annulus and nucleus. Using this approach, we can observe the force conditions of the entire annulus. In this study, we investigated the pressure change and biomechanical characteristics of each spinal level of the upper thoracic spine in immature pigs during vertical load, 5° of anterior flexion, 5° of posterior extension, and 5° of lateral bending using pressure-sensitive film. Our experiments provide certain reference value for the researchers to study disc pressure of upper thoracic spine.

In conclusion, the findings suggest that the posterior thoracic vertebral structure plays an important role in the motion of the upper thoracic vertebral segment and pressure distribution. During lateral bending, the concave side stress at the annulus of the upper thoracic spine increase obviously, suggesting that asymmetrical stress is a contributory factor for scoliosis progression. Gravity is also an import factor affecting scoliosis progress.

Acknowledgements We thank Changlin Han for providing experiment site and biomechanical test machine.

Funding The study was approved by the Key Project of Medical Scientific Research of Hebei Province (No. 20180611) and Key Research and Development Plan of Hebei Province (No. 18277745D). The funder had no role in study design, data collection and analysis, decision to publish, or preparation of the manuscript.

Compliance with ethical standards

Conflict of interest The authors declare that they have no conflict of interest.

Ethical approval The experimental tests on animals were in compliance with the requirements of the Ethics Committee of the Children's Hospital of Hebei Province.

References

1. Shakil H, Iqbal ZA, Al-Ghadir AH (2014) Scoliosis: review of types of curves, etiological theories and conservative treatment. J Back Musculoskelet Rehabil 27:111–115
2. Lowe TG, Edgar M, Margulies JY, Miller NH, Raso VJ, Reinker KA, Rivard CH (2000) Etiology of idiopathic scoliosis: current trends in research. J Bone Joint Surg (Am Vol) 82:1157–1168
3. Gorman KF, Julien C, Moreau A (2012) The genetic epidemiology of idiopathic scoliosis. Eur Spine J 21:1905–1919
4. de Seze M, Cugy E (2012) Pathogenesis of idiopathic scoliosis: a review. Ann Phys Rehabil Med 55:128–138
5. Perdriolle R, Becchetti S, Vidal J, Lopez P (1993) Mechanical process and growth cartilages. Essential factors in the progression of scoliosis. Spine (Phila Pa 1976) 18:343–349
6. Stokes IA, Iatridis JC (2004) Mechanical conditions that accelerate intervertebral disc degeneration: overload versus immobilization. Spine (Phila Pa) 29:2724–2732
7. Neidlinger-Wilke C, Galbusera F, Pratsinis H, Mavrogonatou E, Mietsch A, Kletsas D, Wilke HJ (2014) Mechanical loading of the intervertebral disc: from the macroscopic to the cellular level. Eur Spine J 23(Suppl 3):S333–S343
8. Edwards WT, Ordway NR, Zheng Y, McCullen G, Han Z, Yuan HA (2001) Peak stresses observed in the posterior lateral anulus. Spine (Phila Pa 1976) 26:1753–1759
9. McMillan DW, McNally DS, Garbutt G, Adams MA (1996) Stress distributions inside intervertebral discs: the validity of experimental "stress profilometry'. Proc Inst Mech Eng 210:81–87
10. Nachemson AL, Disc pressure measurements. Spine (Phila Pa 1976) 1981; 6:93–107.
11. Gay RE, Zhao KD, Ilharreborde B, Bridges J, An K-N (2006) The reliability of intradiscal stress profilometry in cadaveric lumbar discs. J Musculoskelet Res 10:163–171
12. Xu G, Fu X, Du C, Ma J, Li Z, Tian P, Zhang T, Ma X (2014) Biomechanical comparison of mono-segment transpedicular fixation with short-segment fixation for treatment of thoracolumbar fractures: a finite element analysis. Proc Inst Mech Eng 228:1005–1013
13. Germaneau A, Saget M, Vendeuvre T, Doumalin P, Dupre JC, Bremand F, Hesser F, Maxy P, Rigoard P (2014) Biomechanical analysis of spinal instrumentation systems dedicated to stabilise thoracolumbar fractures: comparison between standard open surgical instrumentation and percutaneous techniques. Comput Methods Biomech Biomed Eng 17(Suppl 1):72–73

14. O'Connell GD, Jacobs NT, Sen S, Vresilovic EJ, Elliott DM (2011) Axial creep loading and unloaded recovery of the human intervertebral disc and the effect of degeneration. J Mech Behav Biomed Mater 4:933–942
15. Panagiotacopulos ND, Pope MH, Bloch R, Krag MH (1987) Water content in human intervertebral discs. Part II. Viscoelastic behavior. Spine (Phila Pa 1976) 12:918–924
16. Jiang Y, Sun X, Peng X, Zhao J, Zhang K (2017) Effect of sacral slope on the biomechanical behavior of the low lumbar spine. Exp Ther Med 13:2203–2210
17. Anderson DE, Mannen EM, Tromp R, Wong BM, Sis HL, Cadel ES, Friis EA, Bouxsein ML (2018) The rib cage reduces intervertebral disc pressures in cadaveric thoracic spines by sharing loading under applied dynamic moments. J Biomech 70:262–266
18. Zhang H, Hu X, Wang Y, Yin X, Tang M, Guo C, Liu S, Wang Y, Deng A, Liu J, Wu J (2013) Use of finite element analysis of a Lenke type 5 adolescent idiopathic scoliosis case to assess possible surgical outcomes. Comput Aided Surg 18:84–92
19. Rohlmann A, Zander T, Burra NK, Bergmann G (2008) Flexible non-fusion scoliosis correction systems reduce intervertebral rotation less than rigid implants and allow growth of the spine: a finite element analysis of different features of orthobiom. Eur Spine J 17:217–223
20. Lafage V, Dubousset J, Lavaste F, Skalli W (2004) 3D finite element simulation of Cotrel-Dubousset correction. Comput Aided Surg 9:17–25
21. Carrier J, Aubin CE, Villemure I, Labelle H (2004) Biomechanical modelling of growth modulation following rib shortening or lengthening in adolescent idiopathic scoliosis. Med Biol Eng Comput 42:541–548
22. Rohlmann A, Richter M, Zander T, Klockner C, Bergmann G (2006) Effect of different surgical strategies on screw forces after correction of scoliosis with a VDS implant. Eur Spine J 15:457–464
23. Healy AT, Lubelski D, Mageswaran P, Bhowmick DA, Bartsch AJ, Benzel EC, Mroz TE (2014) Biomechanical analysis of the upper thoracic spine after decompressive procedures. Spine J 14:1010–1016
24. Little AS, Brasiliense LB, Lazaro BC, Reyes PM, Dickman CA, Crawford NR (2010) Biomechanical comparison of costotransverse process screw fixation and pedicle screw fixation of the upper thoracic spine. Neurosurgery 66:178–182, (**discussion 182**)
25. Adams MA, McNally DS, Dolan P (1996) 'Stress' distributions inside intervertebral discs. The effects of age and degeneration. J Bone Joint Surg Br 78:965–972
26. Yildiz KI, Isik C, Tecimel O, Cay N, Firat A, Akmese R, Bozkurt M (2013) Use of contact pressure-sensitive surfaces as an indicator of graft tension in medial patellofemoral ligament reconstruction. Arch Orthop Trauma Surg 133:1657–1663
27. Yao QQ, Zheng SN, Cheng L, Yuan P, Zhang DS, Liao XW, Xu Y, Wang LM (2010) Effects of a new shape-memory alloy interspinous process device on pressure distribution of the intervertebral disc and zygapophyseal joints in vitro. Orthopaedic Surg 2:38–45
28. Kim S, Carl Miller M (2016) Validation of a finite element humeroradial joint model of contact pressure using fuji pressure sensitive film. J Biomech Eng 138(1):014501
29. Petersen SA, Bernard JA, Langdale ER, Belkoff SM (2016) Autologous distal clavicle versus autologous coracoid bone grafts for restoration of anterior-inferior glenoid bone loss: a biomechanical comparison. J Shoulder Elbow Surg 25:960–966
30. Cil A, Yazici M, Daglioglu K, Aydingoz U, Alanay A, Acaroglu RE, Gulsen M, Surat A (2005) The effect of pedicle screw placement with or without application of compression across the neurocentral cartilage on the morphology of the spinal canal and pedicle in immature pigs. Spine (Phila Pa 1976) 30:1287–1293
31. Zhang H, Sucato DJ (2008) Unilateral pedicle screw epiphysiodesis of the neurocentral synchondrosis. Production of idiopathic-like scoliosis in an immature animal model. J Bone Joint Surg (Am Vol) 90:2460–2469
32. Yazici M, Pekmezci M, Cil A, Alanay A, Acaroglu E, Oner FC (2006) The effect of pedicle expansion on pedicle morphology and biomechanical stability in the immature porcine spine. Spine (Phila Pa 1976) 31:E826–E829
33. Zhang Z-M, Su F, Zhang C-L, Ma P-P, Zhang Y, Zhang X-P (2013) The effect of different lumbar segmental fixation on lumbar activity and intervertebral pressure. Chongqing Yi Xue 42:3403–3404
34. McAfee PC, Yuan HA, Fredrickson BE, Lubicky JP (1983) The value of computed tomography in thoracolumbar fractures. An analysis of one hundred consecutive cases and a new classification. J Bone Joint Surg (Am Vol) 65:461–473
35. Adams MA, May S, Freeman BJ, Morrison HP, Dolan P (2000) Effects of backward bending on lumbar intervertebral discs. Relevance to physical therapy treatments for low back pain. Spine (Phila Pa 1976) 25:431–437
36. Steffen T, Baramki HG, Rubin R, Antoniou J, Aebi M (1998) Lumbar intradiscal pressure measured in the anterior and posterolateral annular regions during asymmetrical loading. Clinical Biomech (Bristol, Avon) 13:495–505
37. Mente PL, Stokes IA, Spence H, Aronsson DD (1997) Progression of vertebral wedging in an asymmetrically loaded rat tail model. Spine (Phila Pa 1976) 22:1292–1296
38. Stokes IA, Aronsson DD (2001) Disc and vertebral wedging in patients with progressive scoliosis. J Spinal Disord 14:317–322
39. Stokes IA, Spence H, Aronsson DD, Kilmer N (1996) Mechanical modulation of vertebral body growth Implications for scoliosis progression. Spine (Phila Pa 1976) 21:1162–1167
40. Mente PL, Aronsson DD, Stokes IA, Iatridis JC (1999) Mechanical modulation of growth for the correction of vertebral wedge deformities. J Orthop Res 17:518–524